Interhemispheric Asymmetries in Magnetosphere and Ionosphere Magnetic Field Residuals between Swarm Observations and Earth Magnetic Field Models

Yining Shi[1] and Mark B. Moldwin[1]

[1]University of Michigan, Climate and Space Sciences and Engineering, Ann Arbor, Michigan, USA.

Corresponding author: Yining Shi (yining@umich.edu)

Key points:

- Comparison between Swarm magnetic field vector observations and Earth magnetic field models.
- Statistical magnetic field residual maps show largest differences in high latitude region and around the South Atlantic Anomaly.
- More frequent occurrence of large magnetic field residual under high geomagnetic activity levels in southern hemisphere.

This is the author manuscript accepted for publication and has undergone full peer review but has not been through the copyediting, typesetting, pagination and proofreading process, which may lead to differences between this version and the Version of Record. Please cite this article as doi: 10.1029/2021JA030190.

1. Abstract

We present a statistical study of magnetic field vector residual between Swarm observations and two Earth magnetic field models: the 13th generation International Geomagnetic Reference Field (IGRF) model and the CHAOS-7 model. Statistics of these residuals are important for estimating potential errors for satellite operations when using Earth magnetic models as a reference, as well as for magnetosphere-ionosphere-thermosphere (MIT) studies examining energy input into the system. Magnetic field residuals are calculated as vector differences between observations and model estimation at Swarm satellite positions from 2014 to 2020. Magnetic field residuals for both models increase as geomagnetic activity level increases, and the largest magnitude of vector difference can be around 1800 nT with relatively small angle differences. The CHAOS-7 model shows lower magnetic field residuals compared to IGRF-13. North-south hemispheric asymmetries are seen in magnetic field residuals for high Kp values larger than 6 with the southern hemisphere (SH) having more frequent occurrence of magnetic field residuals larger than 300 nT, especially during SH summer. Most large residual values appear in the high-latitude region with SH seeing additional large residuals around the South Atlantic Anomaly (SAA) region. Midnight and noon sectors show the strongest interhemispheric asymmetries. The northern hemisphere (NH) shows more frequent occurrence of large residuals above 75° magnetic latitude throughout all local times compared to the SH. Identifying asymmetries in large magnetic residuals under high geomagnetic activity levels is helpful for studying the difference in response to ionospheric disturbances in the two hemispheres.

2. Introduction

The Earth's magnetic field mainly consists of two major parts. The internal magnetic field is generated by the Earth's core and crust and is close to a dipole with a tilt and offset. In addition to the internal field, Earth's magnetic field is also affected by external sources from the interaction with the solar wind. The Earth's magnetic field is an essential part of space weather and magnetosphere-ionosphere studies. A fundamental aspect of geomagnetism and space physics efforts has been to measure the Earth's magnetic field as well as model it for better understanding of the structure and dynamics of the internal field and the magnetic field changes due to solar wind energy coupling.

Space-based Earth magnetic field measurements have increased over the years from single satellite to global constellations, such as the early TRIAD satellite (e.g., Iijima & Potemra, 1978); Dynamics Explorer 2 (e.g., Weimer, 2001); Ørsted and Magsat satellites (e.g., Papitashvili et al., 2002), Space Technology 5 satellites (e.g., Slavin et al., 2008); the CHAMP satellite (e.g., Reigber et al., 2002), the Swarm satellites (e.g., Friis-Christensen et al., 2008) and the Iridium constellation (e.g., Anderson et al., 2000). Increased number of satellites greatly improved Earth magnetic field measurements; however, they cannot provide a global view of the Earth's magnetic field at a given time. Multiple Earth magnetic field models are derived from satellite and ground-based measurements to provide information of Earth's internal and external magnetic fields. They are constantly updated with new measurements and aim to provide a close estimation of Earth's magnetic field at any location and time. Some examples of these models are the International Geomagnetic Reference Field (IGRF) series (Thebault et al, 2015); World Magnetic Model (WMM) series (Maus, 2010); CHAOS model series (Finley et al., 2016); and the Potsdam Magnetic Model of the Earth (POMME) series (Maus et al., 2006). Due to the changing geomagnetic field, the models are usually updated every several months (e.g. CHAOS) to every 5 years (e.g. IGRF).

Most Earth magnetic field models are derived from quiet time magnetic field measurements and estimate the field without strong magnetospheric and ionospheric disturbances. Comparison between modeled magnetic fields and the measurements they are derived from are therefore limited to low geomagnetic activity levels (e.g., Maus et al., 2006, Finlay et al., 2017, Friis-Christensen et al., 2017). Earth magnetic field model estimations are reference for applications such as satellite location and attitude control (e.g., Lerner and Shuster, 1981), therefore it is essential to have knowledge of the potential location and range of error when using a quiet time magnetic field model as reference under high geomagnetic activity conditions. In addition to operational purposes, magnetic field perturbation derived as the difference between satellite magnetic field observations ($\delta\boldsymbol{B} = \boldsymbol{B_0} - \boldsymbol{B}$, where $\boldsymbol{B}$ is the satellite magnetic field measurement and $\boldsymbol{B_0}$ is the background magnetic field (often given by IGRF or CHAOS)) has been used in estimation of Poynting flux in research for several satellite data sets (e.g., Gary et al., 1994, Waters et al., 2004, Knipp et al., 2011, Rodríguez-Zuluaga et al., 2017), which is an important part for the understanding of energy input in the magnetosphere-ionosphere-thermosphere (MIT) coupling. However, only a few studies have looked at the comparison between observations and modeled

field statistically, especially under high geomagnetic activity levels and mostly focused on the low-latitude region (Lühr and Zhou, 2020 and references within).

In this study, we focus on studying the statistical comparison between the Swarm satellites and two Earth field models IGRF-13 and CHAOS-7 under high geomagnetic activity levels for the whole globe. The Swarm satellites provide global coverage of the magnetic field since their launch in 2013. IGRF-13 and CHAOS-7 are chosen because they include different sources of Earth's magnetic field while both used Swarm data to derive their model.

3. Data and Method

The low-Earth orbit (LEO) satellite data used in this study are provided by the Swarm mission supported by the European Space Agency (ESA). The Swarm mission consists of three identical satellites Alpha (A), Bravo (B) and Charlie (C), where satellite A and C fly side-by-side at an altitude of 462 km and 87.35° inclination angle and satellite B flies at an altitude of 511 km and 87.75° inclination angle initially (https://earth.esa.int/eogateway/missions/swarm). Swarm mission Level 1B (L1b) magnetic vector data product (Olsen et al., 2013) with Product Baseline number 05 measured by the Vector Field Magnetometer (VFM) in geocentric north, east, and geocentric-down (NEC) coordinate from November 25th 2013 to December 31st 2020 at a 1-min cadence are used for investigation and denoted as B_{NEC} in this paper. According to Swarm L1b product definitions, B_{NEC} data with flags of 255 indicate not enough VFM samples to generate $\boldsymbol{B}_{NEC}$ and are omitted in the study. The time range covers the declining phase of solar cycle 24 including solar maximum and solar minimum, giving a relatively complete representation of different solar activity levels.

Two Earth magnetic field models are compared to the Swarm observations, the IGRF 13th generation model (Alken et al., 2021) and CHAOS-7 model (Finlay et al., 2020) including the estimation of core, lithosphere and magnetosphere. Both models are derived using magnetic field measurements from LEO satellites such as Ørsted (Neubert et al., 2001), CHAMP (Reigber et al., 2002) and Swarm, as well as ground-based observatories. The residual between Swarm observation and Earth magnetic field models is calculated as the vector magnetic field at Swarm positions $\boldsymbol{B}_{NEC}$ subtracting the magnetic field estimated by the model $\boldsymbol{B}_{IGRF}$ and $\boldsymbol{B}_{CHAOS}$:

$$\boldsymbol{B}_{IGRF\_Residual} = \boldsymbol{B}_{NEC} - \boldsymbol{B}_{IGRF} \quad (1)$$

$$\boldsymbol{B}_{CHAOS\_Residual} = \boldsymbol{B}_{NEC} - \boldsymbol{B}_{IGRF} \quad (2)$$

Magnitude of magnetic field residual is calculated as $|\boldsymbol{B}_{IGRF\_Residual}|$ and $|\boldsymbol{B}_{CHAOS\_Residual}|$. In addition to magnetic field residual vector, the difference in magnitude of observation versus model, as well as the angle between observations and models are calculated as:

$$B_{Swarm-IGRF} = |\boldsymbol{B}_{NEC}| - |\boldsymbol{B}_{IGRF}| \quad (3)$$

$$\theta_{Swarm-IGRF} = \cos^{-1}\left(\frac{\boldsymbol{B}_{NEC}\cdot\boldsymbol{B}_{IGRF}}{|\boldsymbol{B}_{NEC}||\boldsymbol{B}_{IGRF}|}\right) \quad (4)$$

The calculation for the CHAOS model is the same as IGRF.

We use the Python package, viresclient (https://doi.org/10.5281/zenodo.2554162), to access all Swarm L1b measurements, IGRF-13 and CHAOS-7 model estimations from ESA's VirES for Swarm service (https://vires.services).

Since both Earth magnetic field models are largely derived from LEO satellite measurements during geomagnetic quiet time, this study focuses mostly on the observation-model residual under active geomagnetic conditions. The magnetic field vector measurements from Swarm satellites and modeled magnetic field are divided into groups based on the Kp index (Bartels et al., 1939) since the satellite measurements are global. Kp*10 indices are accessed through Swarm VRE and data are grouped in between Kp*10 values of 30, 35, 40, 45, 50, 55, 60, 70, 80, and 90. Kp*10 values higher than 60 have significantly lower occurrence compared to lower than 60, and therefore have widths of 10 instead of 5.

Satellite locations are transferred from geocentric to Altitude-Adjusted Corrected Geomagnetic (AACGM) coordinates (Shepherd, 2014) for all Swarm locations above 40° latitude and Corrected Geomagnetic (CGM) coordinates below 40° latitude (Gustafsson et al., 1992) due to the fact that AACGM cannot convert locations at satellite altitude in the low latitude for further investigation. Northern hemisphere (NH) and Southern hemisphere (SH) are separated in geomagnetic coordinates.

4. Results

We present first an example of Swarm observations and magnetic field residual between Swarm and IGRF in geomagnetic coordinate magnetic local time (MLT) and magnetic latitude (MLAT)

in Figure 1. The horizontal Swarm observations in blue and magnetic field residuals in red are plotted in geomagnetic coordinates for March 22nd, 2015, on which a moderate geomagnetic storm happened, resulting in a median Kp value of about 6 for the day. Also in Figure 1 is a smaller inset plot showing an example of the time series of the residuals in three directions for one polar orbit during the day when Kp just turned 6. Large residuals appear in the high latitude region for both hemispheres but with different directions and magnitude.

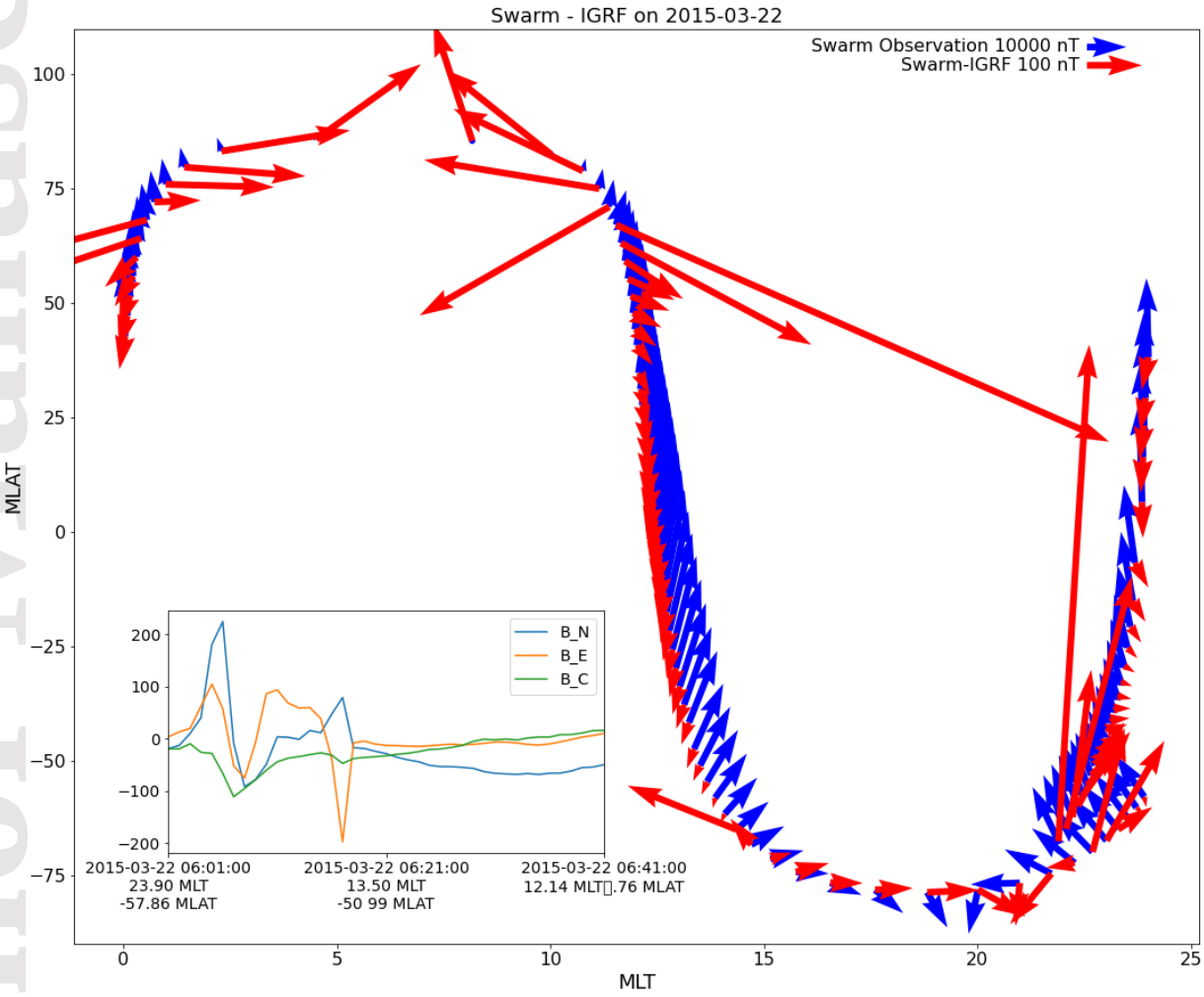

Figure 1. Swarm observations and magnetic field residuals between Swarm and IGRF on March 22nd, 2015.

A statistical view of the magnetic residual between Swarm and Earth magnetic field models for the two hemispheres is shown in Figure 2. Figure 2(a) and 2(b) show the 25%, 50% and 75% quartiles of the magnetic field residual vector magnitude between Swarm and IGRF-13, Swarm

and CHAOS-7 respectively. The two hemispheres are separated with NH quantiles plotted in blue and SH in red.

The magnitude of residual increases with increasing Kp index for both models, which is expected since neither model includes the magnetic field change related to ionospheric disturbances and small-scale magnetospheric disturbances under high geomagnetic activity conditions. The residuals are lower for CHAOS-7 model compared to IGRF-13 model for all Kp values since the CHAOS model includes the magnetic field from the Earth's lithosphere and some external field from large-scale magnetospheric sources such as the ring current and magnetotail and magnetopause currents. The difference of magnetic residuals between the two models ranges from about 30 nT for Kp<6 conditions to as high as about 90 nT for higher Kp levels. A figure of IGRF residuals and CHAOS residuals plotting against each other for the same Kp*10 groups as in Figure 2 is provided in the supplementary material Figure S1 to give a more direct comparison between the two models.

In addition to the expected increase of magnetic field residual, the SH residual is slightly lower compared to the NH for low Kp values and grows higher for large Kp values above 6 even though the two hemisphere quantiles mostly follow the same trend. This slight increase in SH residual quantiles is investigated in the following parts of this paper.

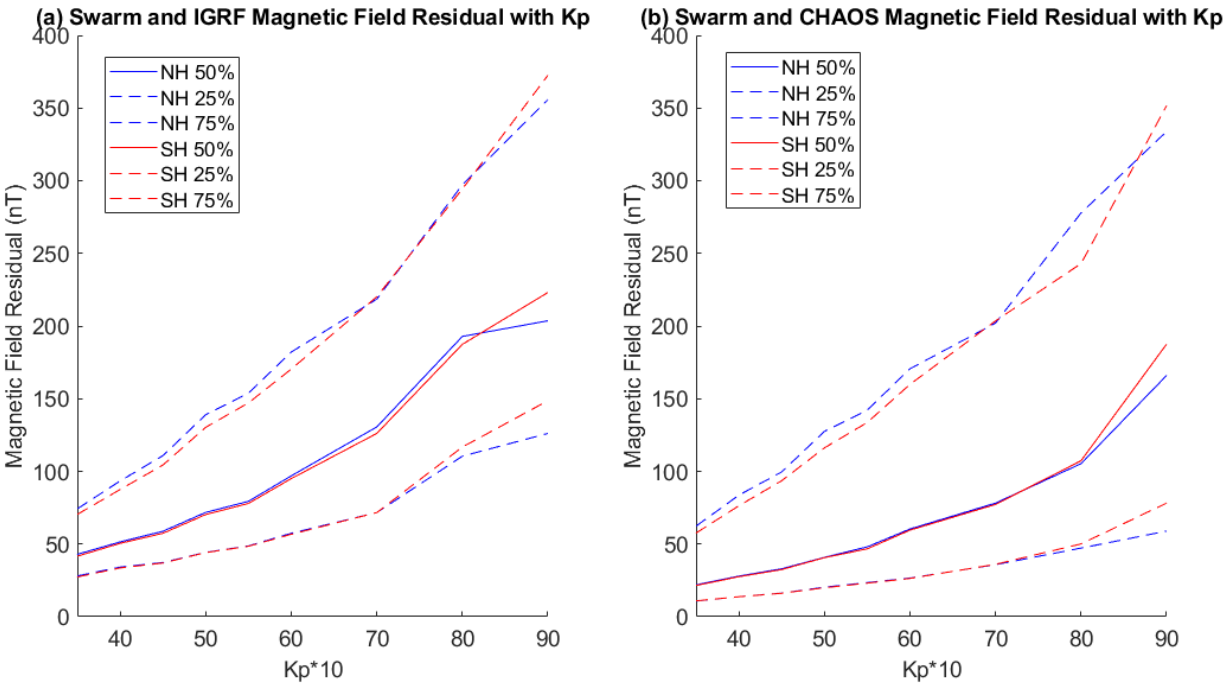

Figure 2: Magnitude of Swarm and Earth magnetic field model residual vectors quartiles as a function of Kp index for (a) IGRF-13 model and (b) CHAOS-7 model.

The largest magnitude of 75% quartiles for the residuals is around 350 nT as shown in Figure 2, which is less than 1% of the Earth's magnetic field. However, the range of magnetic residuals at different latitudes and magnetic local times is relatively large and the statistics of the residuals does not give an accurate view of individual residuals, especially for active geomagnetic conditions, the focus of this study.

To give an example of the larger residuals under active geomagnetic conditions, the magnitude of Swarm and IGRF residuals $|\boldsymbol{B}_{IGRF\_Residual}|$ map for Kp values larger than 6 during equinox months (March-May and September-November) are plotted in geomagnetic coordinates in Figure 3. The same plot for CHAOS is similar to the IGRF plot and provided in the supplementary material Figure S2.

The largest residual is around 1800 nT, much higher than the 75% quantile value. The large residual values mostly appear in the high-latitude region between 55° and 80° for both hemispheres where ionospheric currents unaccounted for in the Earth magnetic models appear during geomagnetic active times. A thin line of data gap is registered around 40° and -40° in the two hemispheres respectively due to change of geomagnetic coordinate from AACGM to CGM, but does not affect the large residual distribution significantly.

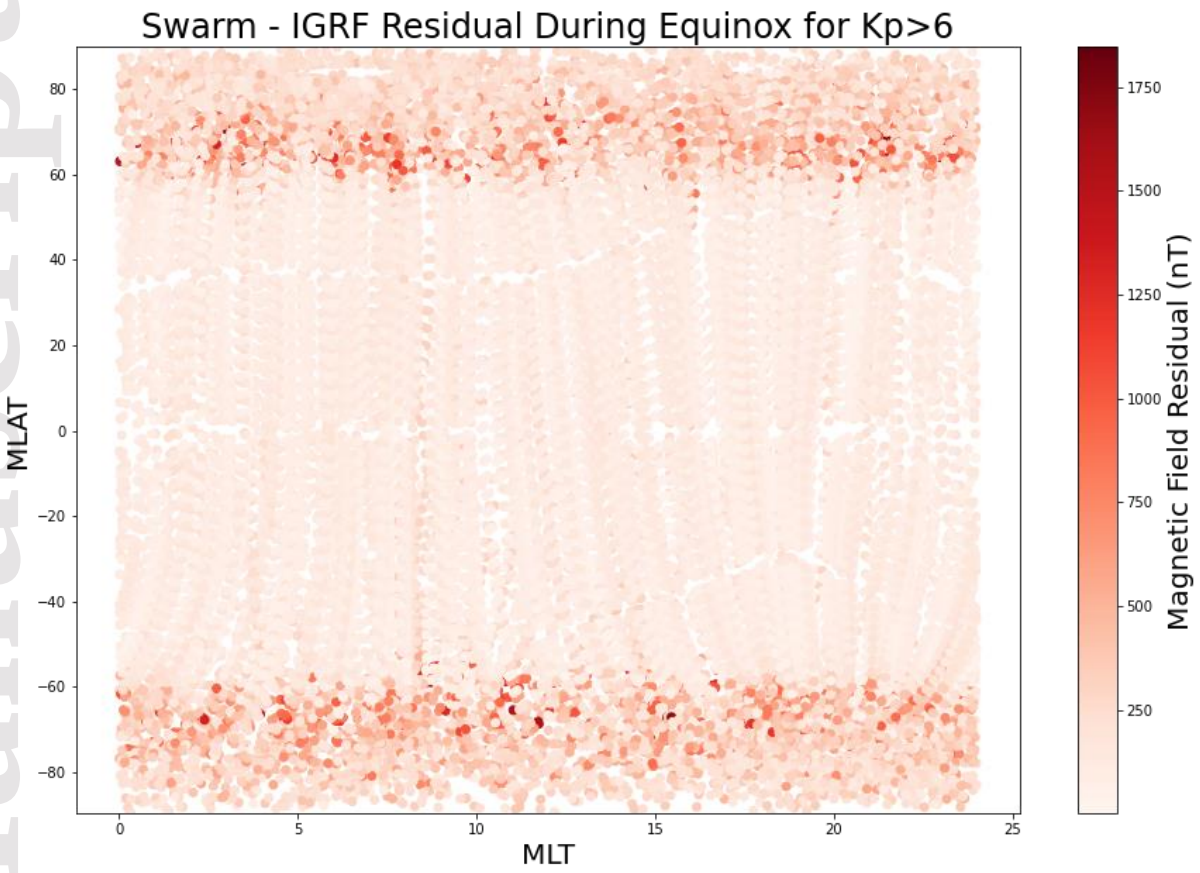

Figure 3: Magnitude of Swarm – IGRF residual vectors map during equinox months for Kp>6 conditions.

To quantify the hemispheric asymmetry seen in the magnetic field residual, the number of $|\boldsymbol{B}_{IGRF\_Residual}|$ and $|\boldsymbol{B}_{CHAOS\_Residual}|$ values larger than 300 nT cases under Kp>6 conditions are counted for the two hemispheres, which accounts for 16.67% of all measurements. Since seasonal effect is well-known for causing inter-hemispheric asymmetry in solar illumination due to the tilt of Earth geographic axis, different seasons are separated. The frequency of large residuals in each hemisphere is calculated as the percentage of residual values larger than 300 nT compared to the total number of measurements in each hemisphere since the two hemispheres have different number of measurements. Table 1 shows the total number of measurements and ratio of residuals larger than 300 nT for both models during different seasons: equinox has the months of March to May and September to November; NH summer has months June to August; and SH summer has months December to February, as well as the ratio of NH percentage over

SH percentage for both geomagnetic field models. A value larger than 1 indicates more NH residual values larger than 300 nT occurred compared to SH and vice versa.

Table 1. NH/SH large residual frequency comparison.

NH Large Residual/Total	Equinox	NH Summer	SH Summer
IGRF-13	2224/13169=0.1689	838/3765=0.2226	410/3719=0.1102
CHAOS-7	2055/13169=0.1560	755/3765=0.2005	375/3719=0.1008
SH Large Residual/Total	Equinox	NH Summer	SH Summer
IGRF-13	2538/14225=0.1784	614/3925=0.1564	837/4021=0.2082
CHAOS-7	2289/14225=0.1609	558/3925=0.1421	797/4021=0.1982
NH/SH	Equinox	NH Summer	SH Summer
IGRF-13	0.9465	1.4228	0.5296
CHAOS-7	0.9686	1.4105	0.5087

We see that the two models show similar results in Table 1. During equinox time, the ratio is slightly less than 1, indicating the SH having slightly more occurrence of large residual values compared to the NH, but the two hemispheres are not statistically different at a 90% confidence level according to calculated z-score (Illowsky and Dean, 2018). However, for solstice periods, the differences between two hemispheres are statistically significant. The ratio of NH/SH or local summer/winter is a bit higher than 1.4 during NH summer, but during SH summer, the SH/NH or local summer/winter ratio is close to 2 (1/0.5296 or 1/0.5087). This result is consistent with seasonal effect of ionospheric disturbances where the summer hemisphere sees larger disturbances compared to the winter (Laundal et al., 2017 and references within), but the SH summer has a significantly higher seasonal asymmetry of large residual occurrence compared to NH summer.

The results presented so far analyzed the magnitude of the residual vector. The vector difference consists of two parts, the difference in magnitude of observations and modeled magnetic fields,

as well as the angle difference between them. These two aspects are investigated separately in this section.

Figure 4 shows the histogram of magnitude difference between Swarm observations and IGRF-13 magnetic field for (a) NH and (b) SH; as well as the histogram of angle difference between the two for (c) NH and (d) SH. To show the larger residual values more clearly, all residuals $|\boldsymbol{B}_{IGRF\_Residual}|$ > 300 nT under Kp>6 conditions during equinox are counted in these plots since large residual values show up more frequently under higher Kp values and the two hemispheres are mostly symmetric under lower Kp values. The winter and summer seasons are omitted since the large residuals under Kp>6 occurrence is different for NH summer and SH summer as shown in Table 1. The same plot for CHAOS-7 model shows similar trends and is provided in the supplementary material Figure S3.

Note that the magnitude difference plotted here is the relative difference calculated as

$$B_{Swarm-IGRF} = \frac{|\boldsymbol{B}_{NEC}| - |\boldsymbol{B}_{IGRF}|}{|\boldsymbol{B}_{IGRF}|} \times 100\%$$

since the magnetic field in the two hemispheres are different and the SH has on average smaller magnetic fields. The absolute difference histograms are provided in the supplementary material Figure S4. The results shown in this study so far have all been comparison of absolute values of residual vectors and the SH residuals relative to their modeled magnetic fields are larger compared to the NH.

In Figure 4(a) and 4(b), majority of the magnitude differences are larger than 0, indicating that the IGRF model is under-estimating the magnetic field most of the time. The SH shows more magnitude differences that are larger than 0.5% compared to NH and the largest difference can be more than 1.5% while the NH does not have such extreme deviations.

In Figure 4(c) and 4(d), we show that the angle differences between Swarm observations and the IGRF model are mostly between 0.5° to 1°. The largest angle difference in the SH can go up to 2.5° while the NH does not show as large an extreme. Both magnitude and angle differences are more likely to be higher in the SH and the largest differences are in the SH as well.

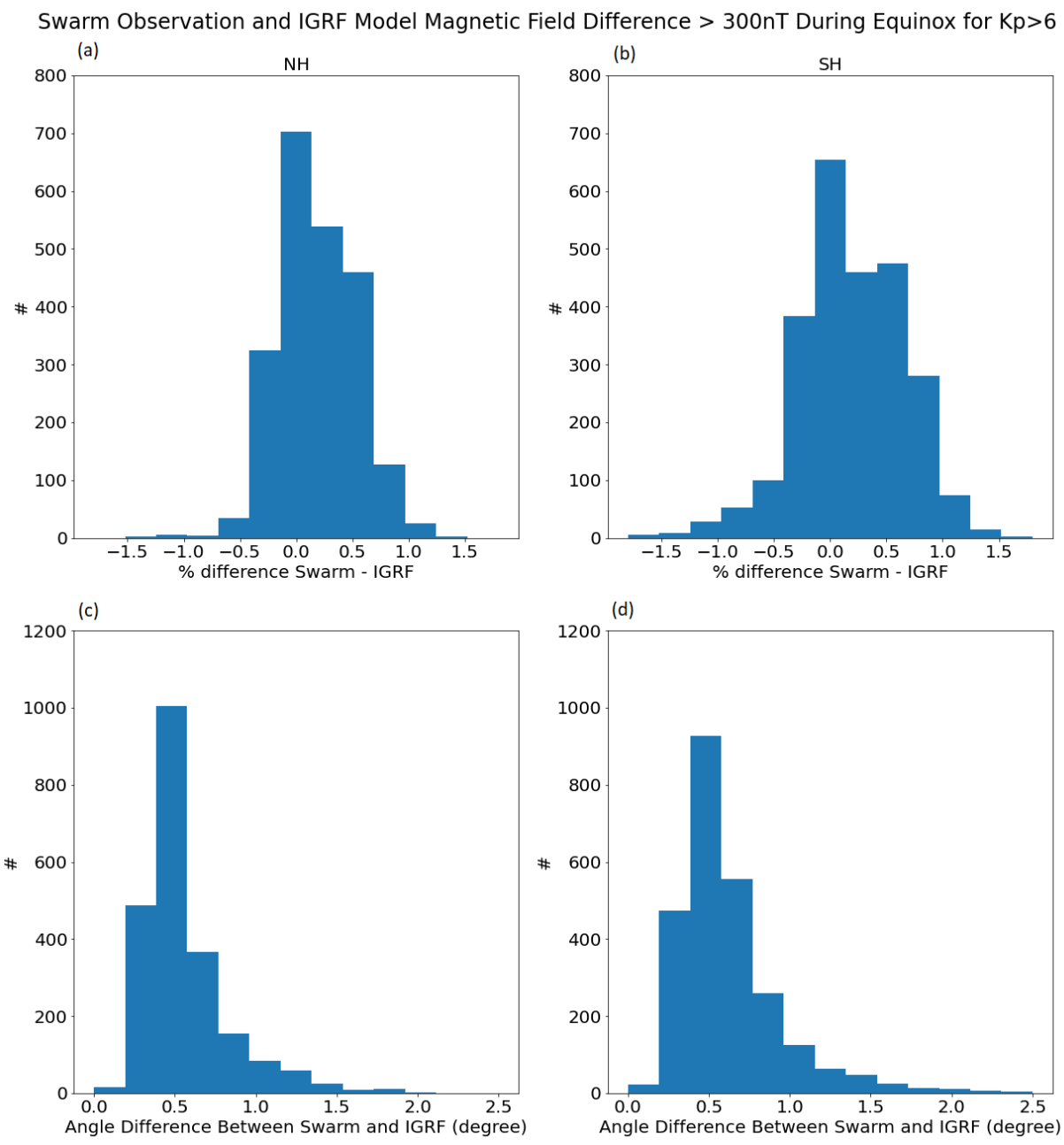

Figure 4. Histogram of Swarm and IGRF relative magnitude difference for (a) NH and (b) SH; angle difference for (c) NH and (d) SH.

5. Discussion

In this section, we look at where the interhemispheric asymmetries show up for the $|\boldsymbol{B}_{IGRF\_Residual}|$ > 300 nT cases under Kp>6 conditions and look for possible geophysical mechanisms to cause the interhemispheric asymmetries for these large residuals.

The first obvious asymmetry shows up in the low-to-mid latitudes around the South Atlantic Anomaly (SAA) where the Earth's magnetic field intensity is particularly low. Figure 5 shows all the $|\boldsymbol{B}_{IGRF\_Residual}|$ > 300 nT cases under Kp>6 conditions in geographical coordinates in a white-to-red color scale. All points with magnetic field intensity less than 25000 nT measured by the SWARM satellites are plotted in contours on the map to indicate the location of SAA in a yellow-to-purple color scale with purple for the lowest values. Also plotted in Figure 5 in black dots are the nightside auroral boundaries in the NH with 1-hr magnetic local time intervals estimated from an empirical model at Kp = 6 (Carbary, 2005). Note that the dayside auroral boundaries are not estimated in the model due to limitation of data selection. Most large residual values appear in the high-latitude regions, but the southern hemisphere has more residual values slightly larger than 300 nT in the low-to-mid latitude region. The residuals appear during multiple orbits around the lowest magnetic field intensity region as well as just outside of the SAA region. Since there are only a few tracks of measurements in the lowest region of magnetic field intensity, we cannot rule out that they're there by coincidence. However, the SAA also results in a clear increase in large residual cases around the -60° geographical latitude, or just below -50° geomagnetical latitude, therefore we believe the large residuals around SAA are not all by coincidence, and one possible reason for the large residuals is the models are not estimating the magnetic field around SAA well enough.

There are very few residual values larger than 300 nT cases around the SAA for the CHAOS model because the residual values for CHAOS model are on average lower than the IGRF model. However, an increase in residual values similar to the results in Figure 5 is still present around the SAA if all residual values larger than 200 nT cases are plotted instead, as shown in the supplementary material Figure S5, similar to Figure 5 but with residual values larger than 200 nT for CHAOS to show the SAA effect.

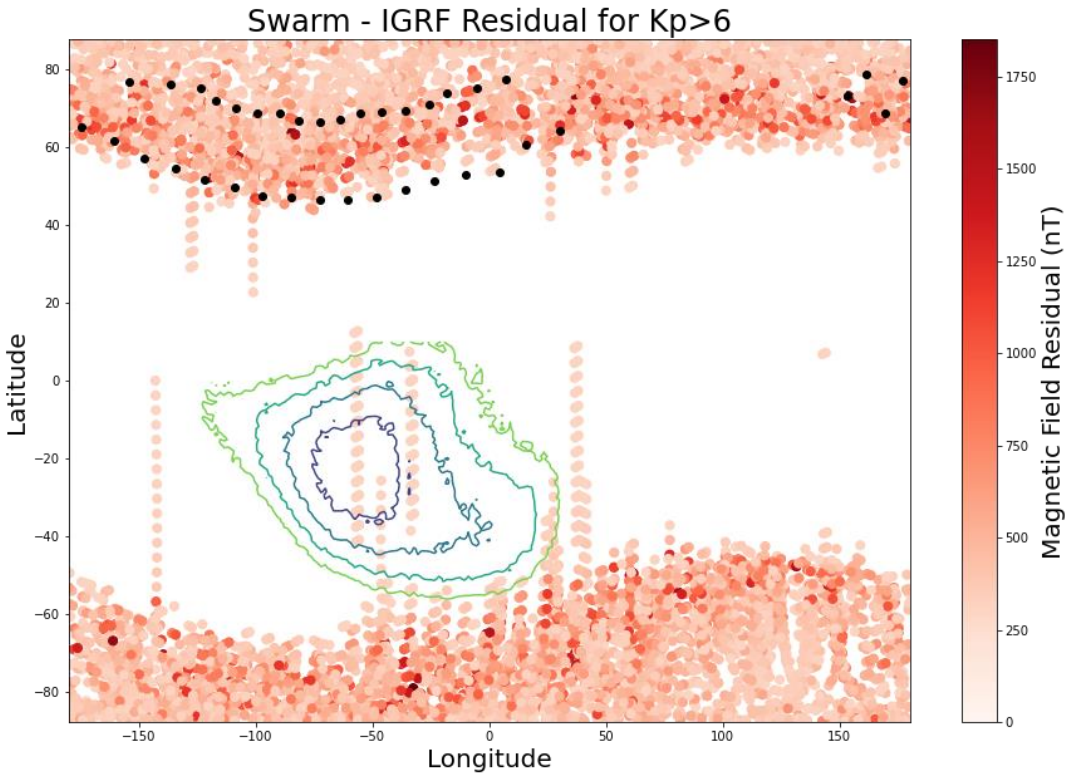

Figure 5: Swarm - IGRF residual values larger than 300 nT cases for Kp>6 conditions in geographical coordinates (white-to-red-dots), SAA region (yellow-to-purple contours) and NH nightside auroral boundaries (black dots).

As shown in Figure 3, most large residual cases appear in the high-latitude region, starting around the equatorward auroral boundary and extending all the way to the poles in both hemispheres, so in this section we only examine the region above 50° latitude in both hemispheres. To statistically test if the two hemispheres have different distributions of large residuals at different magnetic local times (MLT), the proportion of $|\boldsymbol{B}_{IGRF\_Residual}| > 300$ nT percentage over all measurements in each 1-hr MLT bin for latitude higher than 50° is calculated in each hemisphere and compared. Figure 6 shows the frequency of large residual in the two hemispheres. A 90% confidence interval calculated from a z-score of 1.654 and the standard error in the two samples is shown as error bar around the NH ratio for all MLTs. If the SH ratio falls within the 90% confidence interval, it indicates that the ratio difference between the two hemispheres is not large enough based on the sample size for the two hemispheres' large residual frequency to be statistically different (Illowsky and Dean, 2018). All SH ratio statistically the same as NH are indicated in blue and different in red, with SH plotted above the interval

indicating SH having higher frequency of large residuals statistically compared to the NH and if SH is plotted below the interval it indicates that the SH has a lower frequency than the NH statistically.

Similar plot for the CHAOS model is shown in supplementary material Figure S6. The CHAOS model shows similar more frequent occurrence of large residuals around noon though not for all of the MLTs, similar difference between the two hemispheres is also seen on the nightside around the midnight region.

The percentage of large residuals is significantly higher above 50° latitude, which can be as high as 45% of all measurements under Kp>6 conditions at some MLTs. Two regions of statistically significant hemispheric asymmetries are shown in the figure. The SH shows higher frequency of large residuals around the noon region from 8 to 13 MLT. The other region of interhemispheric asymmetry is near midnight where the NH has higher frequency pre-midnight around 21-22 MLT and 3-4 MLT and the SH around 0-1 MLT and 4-5 MLT.

Considering possible sources of large residual values between Swarm and Earth magnetic field models are likely to be currents caused by geomagnetic disturbances, it is expected that large residual values occur frequently in dawn and dusk sectors for both hemispheres where large-scale Region 1 (R1) and Region 2 (R2) field-aligned currents (FACs) are located (e.g., Iijima and Potemra, 1978, Weimer, 2001, Papitashvili et al., 2002).

Asymmetries around noon and midnight sectors are likely due to disturbances from sources other than R1 R2 FACs under high geomagnetic activity. The interhemispheric asymmetries in the Earth's main magnetic field is one possible cause for the more frequent large residual in the SH. The SH has weaker magnetic field intensity and larger offset between geographic and geomagnetic poles compared to the NH (Laundal et al., 2017) and therefore sees more solar insolation and results in greater conductance during summer. Further research is needed to determine the sources of asymmetries due to external disturbances from interaction with the solar wind, but some possible sources are strong small-scale FACs (e.g., Neubert and Christiansen, 2003 and references within) and Alfvén waves (e.g., Chaston et al., 2003 and references within) have been found to be the frequently located in the cusp region and pre-midnight region. High thermospheric density enhancements are also observed in the cusp region, possibly related to small-scale FACs (e.g., Lühr et el., 2004), indicating studies on comparing large residual magnetic

field values to thermospheric density can be helpful to further relate the source of asymmetries to geophysical processes.

To further study the physical processes resulting in asymmetric large residuals in the two hemispheres, solar wind parameters such as interplanetary magnetic field (IMF) By, Bz, solar wind speed and other indices such as Dst and AE for all days with residuals larger than 300 nT (46 days in total) will be studied to identify possible solar wind drivers for the large residuals in a future study.

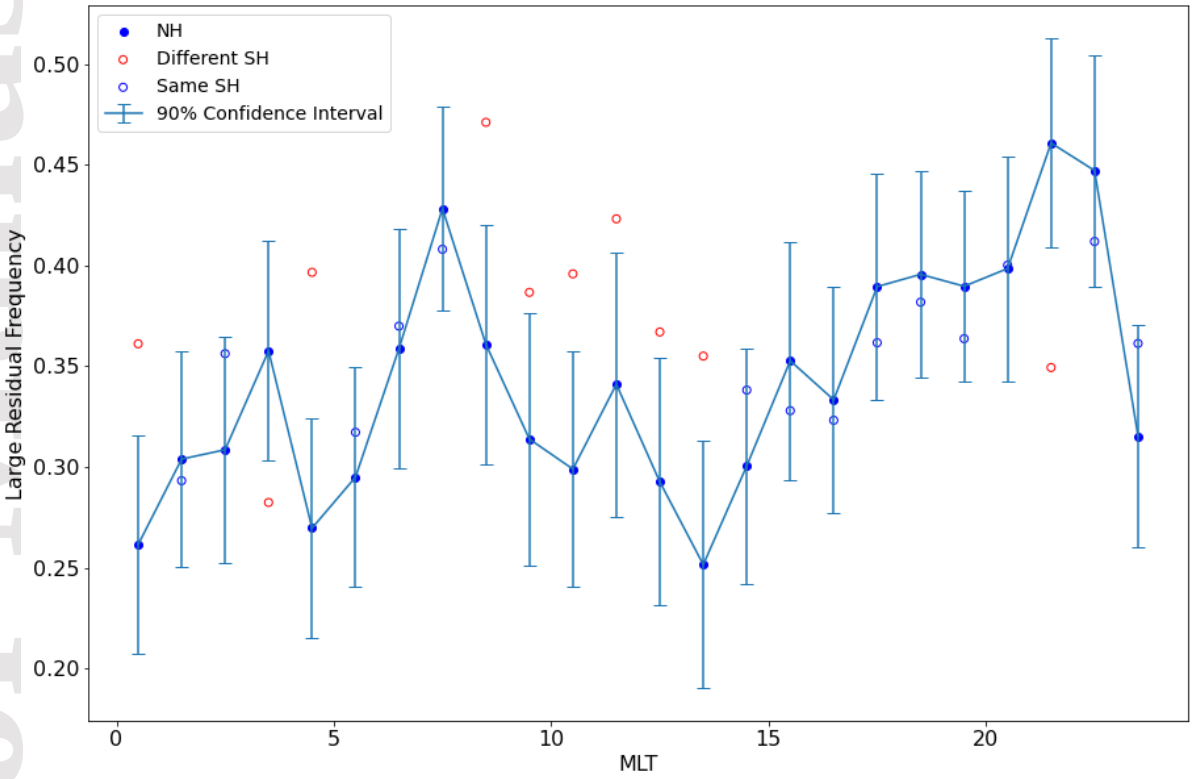

Figure 6: NH and SH frequency of Swarm – IGRF large residuals above 50° and 90% confidence interval of the two hemispheres having the same distribution statistically.

Figure 7(a)-(d) shows the magnetic latitude (MLAT) histogram of all large residual cases in noon sector from 8 to 13 UT for (a) NH and (b) SH, in midnight sector from 21 to 4 UT for (c) NH and (d) SH.

For the MLAT histograms, the distribution in NH and SH differs. The NH shows more frequent large residual occurrence just above 65° with a heavier tail toward higher latitudes and higher

occurrence above 75°, while the SH distribution is more centered around -70° and decreases toward higher and lower latitudes more equally. The MLAT distributions of dawn and dusk are similar to those of noon and midnight and provided in the supplementary material Figure S7, indicating the distribution of large residual values at different latitudes is not closely related to the geomagnetic local time, but consistently different in the two hemispheres. The same trend is found in MLAT distribution histograms for CHAOS residuals as provided in supplementary material Figure S8 and S9. This asymmetry is likely caused by geographical difference of the two hemispheres where the offset between geographic and geomagnetic poles is smaller in NH (Laundal et al., 2017 and references within).

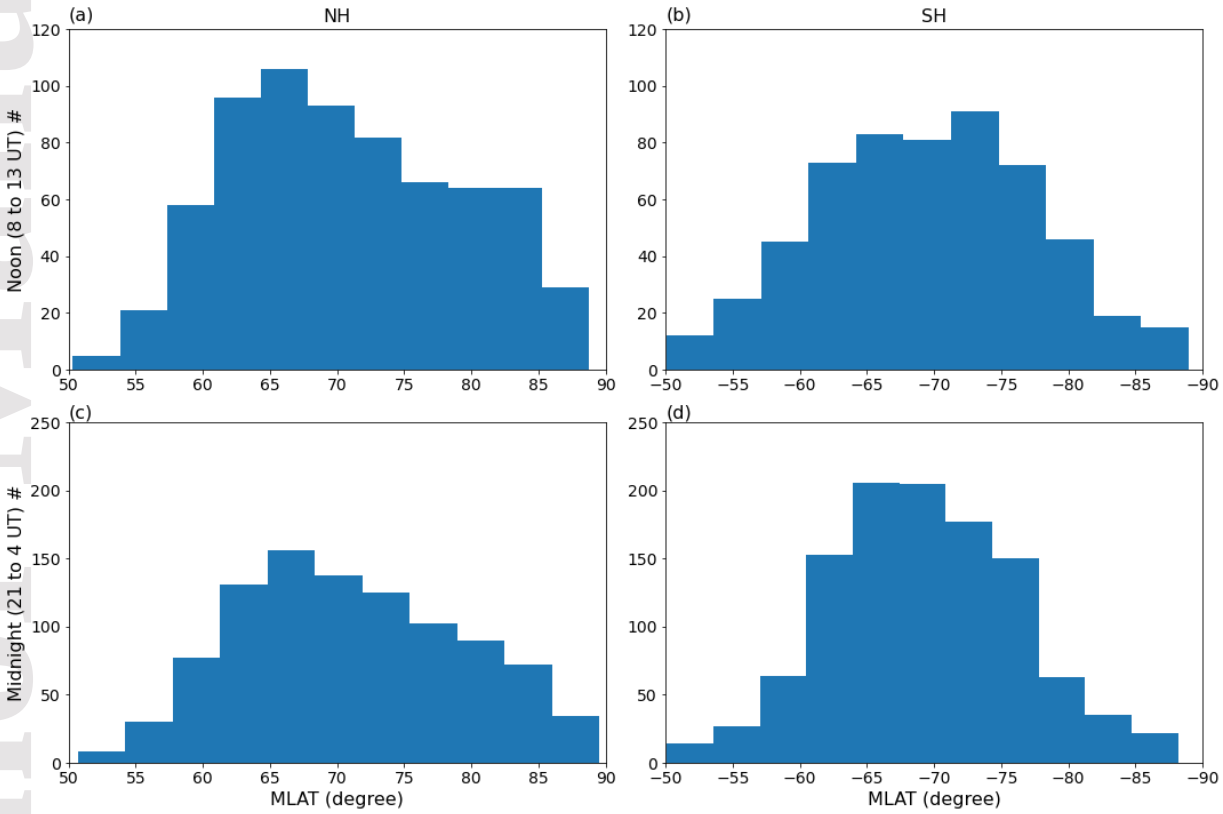

Figure 7: (a)-(d) Magnetic latitude histograms for Swarm – IGRF large residual cases in the NH and SH high-latitude region in noon and midnight sectors.

6. Summary and Conclusions

In this study, we compared Swarm magnetic field vector measurements and estimates of Earth's magnetic field from two Earth magnetic field models: IGRF-13 and CHAOS-7 between the years

2014 and 2020. Residuals between measurements and models are studied to provide a statistical view of the models and highlight ionospheric and magnetospheric current perturbations.

Both Earth magnetic field models show larger residuals with increasing geomagnetic activity level indicated by higher Kp values. CHAOS-7 model residuals are on average 30-40 nT smaller than IGRF-13 model, so CHAOS-7 model would be better for navigation and attitude determination purpose, but both models show very similar distributions for large residual values. Largest residual values can be as high as 1800 nT in the IGRF-13 model and most large residual values appear in the high-latitude region where ionospheric currents occur under high geomagnetic activity levels.

Statistics found for the residuals in this paper can be used as a reference for possible errors when using modeled Earth magnetic field derived from mostly geomagnetic quiet times under high geomagnetic activity levels. The large residuals and their occurrence frequency also demonstrate that relying on geomagnetic field models to estimate DC Poynting flux significantly underestimates the electromagnetic energy flux input into the ionosphere, with residuals larger than 300 nT happening around 16.67% of the time for all satellite orbits and increases to over 45% in the high-latitude region above 50° for some MLTs. If used to estimate energy input through Poynting flux or calculations of field-aligned current intensity, using CHAOS will underestimate the intensity due to it including some external Earth currents in its formulation compared to IGRF.

Interhemispheric asymmetries are found for the residuals under high geomagnetic activity levels when Kp index is higher than 6. Large residual values higher than 300 nT occur more frequently in the southern hemisphere under Kp>6 conditions, southern hemisphere summertime sees the strongest asymmetry where the southern hemisphere large residual occurrence is close to 2 times that observed in the northern hemisphere.

The SAA results in more large residual values in the southern hemisphere near the region with the lowest magnetic field values, as well as the region around the SAA, just below -50° magnetic latitude in the southern hemisphere.

For the high-latitude region where most large residuals appear, the interhemispheric asymmetry is most apparent in the noon and midnight sectors, with SH showing higher frequency of large

residuals around noon from 08 to 13 UT, while midnight region around 21 to 04 UT showing higher frequencies in the two hemispheres at different local times. Dawn and dusk sectors have similar occurrences of large residual values in the two hemispheres likely due to large-scale R1 and R2 FACs under high geomagnetic activity levels.

Magnetic latitude distribution of large residual values is consistently different in the two hemispheres for all magnetic local times where the northern hemisphere sees the highest occurrence of large residuals at a lower latitude and more large residuals at latitudes above 75° compared to the southern hemisphere.

Identifying the magnetic residual asymmetries in the two hemispheres under high geomagnetic activity levels is helpful for studying differences in response to ionospheric disturbances in the two hemispheres. The next step to understand the cause of higher occurrence of large residual values in the southern hemisphere under high geomagnetic activity levels will be relating large residuals to possible sources of magnetospheric and ionospheric disturbances such as various solar wind parameters, geomagnetic indices and geomagnetic storms and substorms.

Acknowledgement

We thank the ESA Swarm mission (https://earth.esa.int/eogateway/missions/swarm/data) and VirES Server (doi:10.5281/zenodo.2554162) for providing the Swarm L1b data and IGRF-13 and CHAOS-7 modeled Earth magnetic field. This study is supported by NASA grants 80NSSC19K0608 and 80NSSC20K1779.

Data containing all Swarm observations and modeled magnetic field used in this study can be found online at https://doi.org/10.7302/wfgt-sz72.

Figure Captions

Figure 1. Horizontal Swarm observations and magnetic field residuals between Swarm and IGRF on March 22nd, 2015.

Figure 2: Magnitude of Swarm and Earth magnetic field model residual vectors quartiles as a function of Kp index for (a) IGRF-13 model and (b) CHAOS-7 model.

Figure 3: Magnitude of Swarm – IGRF residual vectors zemap for during equinox for Kp>6 conditions.

Figure 4. Histogram of Swarm and IGRF relative magnitude difference for (a) NH and (b) SH; angle difference for (c) NH and (d) SH.

Figure 5: Swarm - IGRF residual values larger than 300 nT cases for Kp>6 conditions in geographical coordinates, SAA region and NH auroral boundaries.

Figure 6: (a)-(d) Magnetic latitude and (e)-(h) residual value histograms for large residual cases in the NH and SH high-latitude region in noon and midnight sectors.

Figure 7. Residual MLAT scatter plot for noon (blue) and midnight (red) sectors in high-latitude region for both hemispheres.

Table Captions

Table 1. NH/SH large residual cases comparison.

Reference

Akasofu, S. I. (1964). The development of the auroral substorm. *Planetary and Space Science*, *12*(4), 273-282, doi:10.1016/0032-0633(64)90151-5.

Alken, P., Thébault, E., Beggan, C.D. *et al.* (2021). International Geomagnetic Reference Field: the thirteenth generation. *Earth Planets Space* **73,** 49, doi:10.1186/s40623-020-01288-x.

Anderson, B. J., Takahashi, K., & Toth, B. A. (2000). Sensing global Birkeland currents with Iridium® engineering magnetometer data. *Geophysical Research Letters*, *27*(24), 4045-4048, doi:10.1029/2000GL000094.

Bartels, J., Heck, N. H., & Johnston, H. F. (1939). The three- hour- range index measuring geomagnetic activity. *Terrestrial Magnetism and Atmospheric Electricity*, *44*(4), 411-454, doi:10.1029/TE044i004p00411.

Chaston, C. C., Bonnell, J. W., Carlson, C. W., McFadden, J. P., Ergun, R. E., & Strangeway, R. J. (2003). Properties of small- scale Alfvén waves and accelerated electrons from FAST. *Journal of Geophysical Research: Space Physics*, *108*(A4), doi:10.1029/2002JA009420.

Olsen, N., Friis-Christensen, E., Floberghagen, R., Alken, P., Beggan, C. D., Chulliat, A., ... & Visser, P. N. (2013). The Swarm satellite constellation application and research facility (SCARF) and Swarm data products. *Earth, Planets and Space*, *65*(11), 1189-1200, doi:10.5047/eps.2013.07.001

Finlay, C.C., Kloss, C., Olsen, N. *et al.* (2020). The CHAOS-7 geomagnetic field model and observed changes in the South Atlantic Anomaly. *Earth Planets Space* **72,** 156, doi:10.1186/s40623-020-01252-9.

Finlay, C. C., Lesur, V., Thébault, E., Vervelidou, F., Morschhauser, A., & Shore, R. (2017). Challenges handling magnetospheric and ionospheric signals in internal geomagnetic field modelling. *Space Science Reviews*, *206*(1), 157-189, doi:s11214-016-0285-9.

Finlay, C. C., Olsen, N., Kotsiaros, S., Gillet, N., & Tøffner-Clausen, L. (2016). Recent geomagnetic secular variation from Swarm and ground observatories as estimated in the CHAOS-6 geomagnetic field model. *Earth, Planets and Space*, *68*(1), 1-18, doi:10.1186/s40623-016-0486-1.

Friis-Christensen, E., Finlay, C. C., Hesse, M., & Laundal, K. M. (2017). Magnetic field perturbations from currents in the dark polar regions during quiet geomagnetic conditions. *Space Science Reviews*, *206*(1-4), 281-297, doi:10.1007/s11214-017-0332-1.

Friis-Christensen, E., H. Lühr, D. Knudsen, and R. Haagmans. (2008). Swarm -An Earth Observation Mission investigating Geospace, *Adv. Space Res.*, **41**(1), 210 - 216, doi:10.1016/j.asr.2006.10.008.

Gary, J. B., Heelis, R. A., Hanson, W. B., and Slavin, J. A. (1994), Field-aligned Poynting Flux observations in the high-latitude ionosphere, *J. Geophys. Res.*, *99*(A6), 11417– 11427, doi:10.1029/93JA03167.

Gustafsson, G., N. E. Papitashvili, and V. O. Papitashvili (1992), A revised corrected geomagnetic coordinate system for epochs 1985 and 1990, *J. Atmos. Terr. Phys.*, 54, 1609–1631, doi:10.1016/0021-9169(92)90167-J.

Iijima, T., & Potemra, T. A. (1978). Large- scale characteristics of field- aligned currents associated with substorms. *Journal of Geophysical Research: Space Physics*, *83*(A2), 599-615, doi:10.1029/JA083iA02p00599.

Iijima, T., Fujii, R., Potemra, T. A., & Saflekos, N. A. (1978). Field- aligned currents in the south polar cusp and their relationship to the interplanetary magnetic field. *Journal of Geophysical Research: Space Physics*, *83*(A12), 5595-5603, doi:10.1029/JA083iA12p05595.

Illowsky, Barbara and Dean, Susan, "Introductory Statistics" (2018). *Open Access Textbooks*. 6. https://commons.erau.edu/oer-textbook/6.

Knipp, D., Eriksson, S., Kilcommons, L., Crowley, G., Lei, J., Hairston, M., and Drake, K. (2011), Extreme Poynting flux in the dayside thermosphere: Examples and statistics, *Geophys. Res. Lett.*, 38, L16102, doi:10.1029/2011GL048302.

Laundal, K. M., Cnossen, I., Milan, S. E., Haaland, S. E., Coxon, J., Pedatella, N. M., ... & Reistad, J. P. (2017). North–south asymmetries in earth's magnetic field. *Space Science Reviews*, *206*(1-4), 225-257, doi:10.1007/s11214-016-0273-0.

Lerner, G. M., & Shuster, M. D. (1981). In-flight magnetometer calibration and attitude determination for near-Earth spacecraft. Journal of Guidance and Control, 4(5), 518-522, doi:10.2514/3.56101.

Lühr, H., & Zhou, Y. L. (2020). Residuals to the CHAOS- 6 geomagnetic field model caused by magnetospheric currents during enhanced magnetic activity. *Geochemistry, Geophysics, Geosystems*, *21*(6), doi:10.1029/2020GC008976.

Maus, S., Macmillan, S., McLean, S., Hamilton, B., Thomson, A., Nair, M., & Rollins, C. (2010). The US/UK world magnetic model for 2010-2015.

Maus S, Rother M, Stolle C, Mai W, Choi S, Lühr H, Cooke D, Roth C (2006) Third generation of the Potsdam Magnetic Model of the Earth (POMME). *Geochem Geophys Geosyst*, *7*(7):Q07,008. doi:10.1029/2006GC001269.

Neubert, T., & Christiansen, F. (2003). Small- scale, field- aligned currents at the top- side ionosphere. *Geophysical Research Letters*, *30*(19), doi:10.1029/2003GL017808.

Neubert, T., Mandea, M., Hulot, G., von Frese, R., Primdahl, F., Jørgensen, J. L., Friis-Christensen, E., Stauning, P., Olsen, N., and Risbo, T. (2001), Ørsted satellite captures high-precision geomagnetic field data, *Eos Trans. AGU*, 82(7), 81– 88, doi:10.1029/01EO00043.

Newell, P. T., & Meng, C. I. (1988). The cusp and the cleft/boundary layer: Low- altitude identification and statistical local time variation. *Journal of Geophysical Research: Space Physics*, *93*(A12), 14549-14556, doi:10.1029/JA093iA12p14549.

Papitashvili, V. O., Christiansen, F., & Neubert, T. (2002). A new model of field- aligned currents derived from high- precision satellite magnetic field data. *Geophysical Research Letters*, *29*(14), 28-1, doi:10.1029/2001GL014207.

Reigber, C., Lühr, H., & Schwintzer, P. (2002). CHAMP mission status. *Advances in space research*, *30*(2), 129-134, doi: 10.1016/S0273-1177(02)00276-4.

Rodríguez-Zuluaga, J., Stolle, C., and Park, J. (2017), On the direction of the Poynting flux associated with equatorial plasma depletions as derived from Swarm, *Geophys. Res. Lett.*, 44, 5884– 5891, doi:10.1002/2017GL073385.

Shepherd, S. G. (2014), Altitude-adjusted corrected geomagnetic coordinates: Definition and functional approximations, *J. Geophys. Res. Space Physics*, 119, 7501– 7521, doi:10.1002/2014JA020264.

Slavin, J. A. , Le G., Strangeway R. J., Wang Y., Boardsen S. A., Moldwin M. B., and Spence H. E. (2008), Space Technology 5 multi- point measurements of near- Earth magnetic fields: Initial results, *Geophys. Res. Lett., 35*, L02107, doi:10.1029/2007GL031728.

Thébault, E., Finlay, C. C., Beggan, C. D., Alken, P., Aubert, J., Barrois, O., ... & Zvereva, T. (2015). International geomagnetic reference field: the 12th generation. *Earth, Planets and Space*, *67*(1), 1-19, doi:10.1186/s40623-015-0228-9

Waters, C. L., Anderson, B. J., Greenwald, R. A., Barnes, R. J., & Ruohoniemi, J. M. (2004). High-latitude poynting flux from combined Iridium and SuperDARN data. In *Annales Geophysicae* (Vol. 22, No. 8, pp. 2861-2875). Copernicus GmbH, doi:10.5194/angeo-22-2861-2004.

Weimer, D. R. (2001). Maps of ionospheric field- aligned currents as a function of the interplanetary magnetic field derived from Dynamics Explorer 2 data. *Journal of Geophysical Research: Space Physics*, *106*(A7), 12889-12902, doi:10.1029/2000JA000295.